J. Fluid Mech. (1976), *vol.* 75, *part* 4, *pp.* 721–735
Printed in Great Britain

Vortex shedding from a blunt trailing edge with equal and unequal external mean velocities

By D. R. BOLDMAN, P. F. BRINICH AND M. E. GOLDSTEIN
NASA Lewis Research Center, Cleveland, Ohio 44135

(Received 21 March 1975)

A flow-visualization study has shown that strong Kármán vortices develop behind the blunt trailing edge of a plate when the free-stream velocities over both surfaces are equal and that the vortices tend to disappear when the surface velocities are unequal. This observation provides an explanation for the occurrence and disappearance of certain discrete tones often found to be present in the noise spectra of coaxial jets. Both the vortex formation and the tones occur at a Strouhal number based on the lip thickness and the average of the external steady-state velocities of about 0·2.

Results from theoretical calculations of the vortex formation, based on an inviscid incompressible analysis of the motion of point vortices, were in good agreement with the experimental observations.

1. Introduction

It has been found that the noise produced by a subsonic coaxial jet has certain peculiarities which depend on the ratio of the primary and secondary jet velocities (Olsen, Gutierrez & Dorsch 1973; Olsen & Karchmer 1976). The dependency is most easily described by referring to figure 1, where the power-level noise spectra for a coaxial nozzle are shown for various ratios of secondary to primary air velocity. The feature of interest to the present investigation is the spike of narrow-band, high frequency noise that occurs at the higher velocity ratios and which decreases as the velocity ratio is reduced. This noise finally disappears into the jet broad-band noise at velocity ratios below 0·5. The Strouhal number for this narrow-band noise based on the thickness of the lip separating the two streams is approximately 0·2, which suggests the presence of a Kármán vortex street emanating from this lip.

The purpose of this investigation therefore was to study the flow in the wake region of a blunt trailing edge, particularly as it relates to the generation of a Kármán vortex street, having either equal or unequal velocities over the top and bottom surfaces of a flat plate. Such a flow is believed to be a reasonable simulation of the interaction between coaxial jets. Further, it is hoped to establish a rational explanation of the observed lip noise phenomena based on established

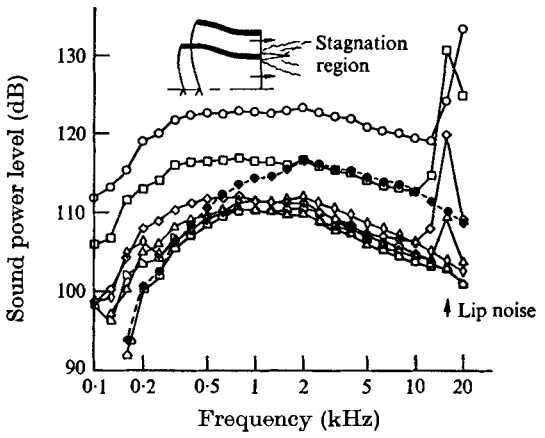

FIGURE 1. Coaxial-nozzle lip noise (from Olsen *et al.* 1973). Core velocity, 244 m/s; core diameter, 5·28 cm; area ratio, 5·4; lip thickness, 0·25 cm. Free-field lossless data.

	○	□	◇	△	⏢	⌂	◊	●
Ratio of secondary to primary velocity	1·0	0·8	0·6	0·5	0·4	0·3	0·2	0

fluid-mechanical behaviour. Although the primary air flow in the noise experiments described by Olsen *et al.* (1973) was 244 m/s, the velocities in the present experiment were reduced by a factor of 10 in order to use smoke visualization techniques to study the vortex development in the wake. However the Reynolds number was approximately the same in the two cases.

2. Apparatus and instrumentation

As indicated in figure 2, the Kármán vortex street was produced downstream of the blunt trailing edge of a flat plate installed in a 9·8 × 25·4 cm wind tunnel at Lewis Research Center. The plate was 79 cm long (excluding the faired leading edge, which extended forward 2·5 cm), 9·8 cm wide and 1·3 cm thick. The width of the forward half of the plate was contoured to fit the entrance bell mouth, and it was this part that served to attach the plate to the tunnel structure. The downstream half of the plate was supported between the glass walls of the tunnel by friction. Elastic seals between the plate and the tunnel walls prevented leakage of air from the top to the bottom of the plate.

A single layer of steel window screening (18 mesh) was sandwiched between the steel bell-mouth flange and the wood fairing, and likewise between the forward edge of the plate and the leading-edge fairing. This screening served to hold the various layers of cloth which were placed in the lower half of the inlet to vary the ratio of the flow velocity over the lower surface to that over the upper surface between zero and unity.

Instrumentation on the flat-plate model consisted of two static-pressure taps 2·5 and 22·9 cm upstream of the trailing edge along the centre-line on the top of the plate and two similarly placed taps on the lower surface of the plate. Upper and lower tunnel wall static-pressure taps were in line with the plate static-

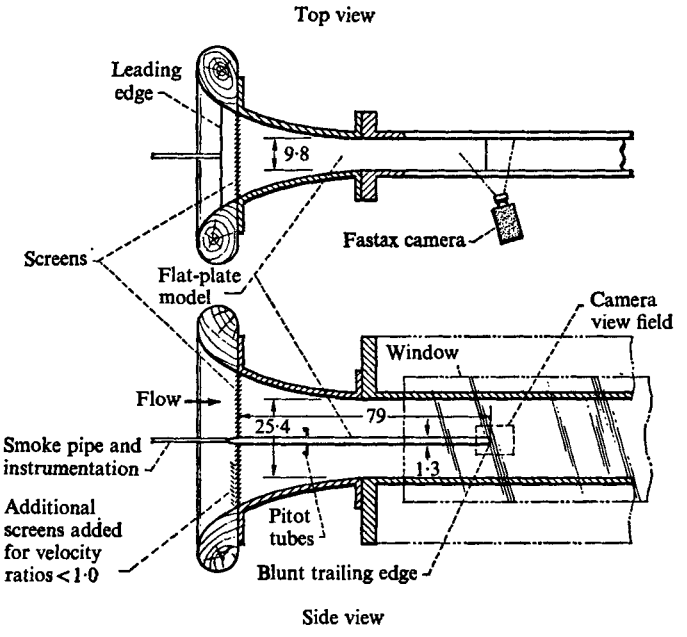

FIGURE 2. Schematic diagram of wind tunnel with plate installed.

pressure taps. An additional static-pressure tap was located on the blunt base. Two Pitot tubes were installed along the centre-line of the plate 20·3 cm downstream of the screen on the upper and lower surfaces as shown in figure 2. A 0·76 cm I.D. tube extended the full length of the model and was used to supply smoke for visualization of the flow in the wake region. The centre of this tube was offset 0·76 cm from the spanwise centre-line of the model and the base static-pressure tap was offset an equal amount on the other side of the model centre-line. The smoke tube and the model pressure instrumentation leads extended straight ahead of the leading edge for 30 cm before making a lateral turn towards the smoke generator and the manometer.

The smoke was generated by burning cigars in an apparatus similar to that described by Herzig, Hansen & Costello (1954) except that the cigars were not soaked in oil as suggested in the reference. Instead, it was found that a cigar moistened with water provided sufficiently dense smoke for photographic purposes. A 16 mm high-speed motion-picture camera was used to photograph the flow in the base region. The camera was operated at about 2300 frames/s and covered a field of view of about 7·6 × 10·2 cm as shown in figure 2. It was directed to give a slightly oblique view of the trailing edge as indicated in the top view in figure 2 and the enlarged photo in figure 3(*a*) (plate 1).

Plate boundary layers were measured immediately upstream of the trailing edge using flattened boundary-layer Pitot tubes. Wake velocity and turbulent intensity profiles were measured at 2·5 and 7·6 cm downstream of the plate trailing edge, using single-element hot-wire probes. All of the above surveys were made along the plate centre-line.

In order to be assured of a turbulent boundary layer over the plate, a strip of no. 180 abrasive paper 5·7 cm long and spanning the width of the plate was attached to the upper and lower surfaces of the plate 28 cm upstream of the trailing edge.

3. Experimental results

The experiment was performed with a fixed free-stream velocity $U_1 = 24{\cdot}4$ m/s over the upper surface of the plate and with several velocities U_2 on the lower surface giving ratios of lower to upper velocity of 0, 0·25, 0·50, 0·75 and 1·0. The stream velocity of 24·4 m/s represents an upper limit to visualization of the vortex-cloud smoke patterns. At lower velocities the vortex-cloud smoke patterns became more distinct, but difficulty in throttling the airstream precluded operation at the lower levels. To the unaided eye the smoke pattern behind the trailing edge resembled a steady wake flow. Use of a stroboscopic light did not change matters much: vortex-cloud patterns still could not be seen. However, use of a high speed motion-picture camera operating at 2300 frames/s revealed the vortex shedding in sufficient detail so that the shedding frequency, vortex-cloud velocity and wake divergence could be measured.

Figures 3 (*b*)–(*f*) (plate 1) are 2 × enlargements of selected motion-picture frames which show some of the differences which occur as the velocity ratio is changed from unity to zero. To clarify these photographs for the reader, a 6 × enlarged, slightly retouched photograph which indicates more clearly what the movie frames represent is presented in figure 3 (*a*). It is generally conceded that a single or even a collection of single frames from high-speed motion pictures of a periodic phenomenon is an inadequate substitute for the film viewed with a good movie projector, since the lack of clarity in a single frame is compensated by the advantage of being able to detect motion. Another problem is that there may be no typical frame or frames, i.e. the phenomenon may not be steady over long periods of time. Thus, in some of the present movie films a well-defined vortex-cloud pattern may exist for a while but at another time be relatively poorly defined. Bearing these considerations in mind, the descriptions of the vortex shedding which follow should be regarded as referring to the typical behaviour of the flow. When the velocity ratio was unity (figure 3*b*) a sequence of well-defined vortex clouds was shed from the top and bottom edge of the plate in such a way that a bottom cloud was positioned midway between two top clouds and vice versa. This is the classical vortex shedding phenomenon usually referred to as a Kármán vortex street. It is known to occur in the Reynolds number range from 300 to 10^5 for turbulent flow (Abernathy & Kronauer 1962). The Reynolds number based on the trailing-edge thickness and the upper air velocity was 2×10^4 in the present study. The wake's total divergence angle measured on a movie screen was about 20°, the vortex shedding rate was about 375 Hz, and the vortex velocity was around 17·4 m/s. Both the upper and the lower vortex clouds appeared to be of equal strength.

Figure 3 (*c*) shows a sequence taken when the velocity ratio was 0·75 (the flow over the lower surface was reduced). The predominant change in this picture

is that the bottom vortex clouds are no longer midway between the top clouds, but tend to be overtaken by the upper ones and are less well defined. The shedding rate of the upper clouds is reduced to 325 Hz, the vortex velocity is 14·6 m/s, and the divergence angle remains at 20°. As the velocity ratio was reduced to 0·5 (figure 3*d*) the shedding rate dropped to 315 Hz, the vortex velocity was about 15·2 m/s, and the divergence angle of the wake reduced to 6°. For this condition the vortex clouds off the lower surface appeared to be much weaker and were overtaken very quickly by the upper ones. The vortex clouds from the upper surface were also less distinct.

At a velocity ratio of 0·25 (figure 3*e*) only vortex clouds from the upper surface could be seen. These were shed at a rate of about 350 Hz and were so indistinct they they were very difficult to detect (hot-wire measurements using a narrow-band wave analyser indicated no predominant shedding frequency). The vortex-cloud velocity could not be estimated because the clouds were too poorly defined. When the velocity ratio was reduced to zero (figure 3*e*) vortices having a characteristic frequency could not be detected and the wake appeared as a succession of random eddies. For both the 0·25 and zero velocity ratios very little spreading of the wake took place in the region of observation. The hot-wire measurements tend to confirm that the gradual loss of clarity of the vortex clouds is due to a local increase in randomness and not to a change in phase of the vortex shedding that may occur along the span.

Boundary-layer velocity profiles measured immediately upstream of the trailing edge were typically turbulent for all the flow conditions down to a velocity ratio of 0·41. Since boundary-layer profiles below this velocity ratio were not measured it cannot be definitely stated that they were turbulent. However, at a velocity ratio of 0·25 (velocity = 6 m/s), the Reynolds number based on plate length is $3{\cdot}2 \times 10^5$ along the lower surface, which is near the lower limit for turbulent flow to exist (Schlichting 1960, p. 37). The presence of the sandpaper roughness upstream on the plate may then be sufficient to ensure turbulent flow at this condition.

Hot-wire surveys of the velocity and turbulent intensity in the wake region were obtained at $x = 2{\cdot}5$ cm downstream of the trailing edge for velocity ratios of 1·0, 0·75, 0·5, 0·25 and 0 and at $x = 7{\cdot}6$ cm for velocity ratios of 1·0, 0·75, 0·31 and 0. In general these profiles indicated a thinning of the wake as the velocity ratio was reduced. This thinning was noted in both the steady-state velocity profiles and the turbulent intensity profiles and agrees qualitatively with the wake thinning noted in the vortex-street motion pictures mentioned earlier.

Shedding frequencies at a distance of 2·5 cm downstream of the trailing edge were also measured with the hot-wire apparatus and a frequency analyser. These results are compared with the previously mentioned results from the movie film in table 1.

Agreement is quite good between the hot-wire measurements of shedding frequency and the results derived from the movie film. The observed trend of decreasing shedding frequencies at velocity ratios $0{\cdot}5 \leqslant U_r \leqslant 1{\cdot}0$ would be expected if the Strouhal number is based on the average of the velocities for the top and bottom of the plate.

	Shedding frequency (Hz)	
$U_r = U_2/U_1$	Hot-wire measurements	Movie-film measurements
1·0	370	375
0·75	325	325
0·5	320	315
0·25	None detected	350?
0	None detected	None detected

TABLE 1. Vortex shedding frequencies

The results of the present vortex-shedding experiment are in good agreement with the acoustic measurements taken by Olsen *et al.* (1973) and Olsen & Karchmer (1976) in coaxial jets even though the test velocity differed by an order of magnitude. Thus, at a velocity ratio of unity Olsen *et al.* (1973) found that the frequency of the lip noise tone was 20000 Hz at a stream velocity of 244 m/s and lip thickness of 0·254 cm. For these conditions the Strouhal number defined as $St = fh/U$, where f = shedding frequency, h = lip thickness, and U = stream velocity, was 0·21. In the present vortex-shedding experiment the frequency was 375 Hz, the velocity was 24·4 m/s, and the trailing-edge thickness was 1·27 cm. For these conditions the Strouhal number is 0·20.

As the velocity ratio was reduced below unity there was a slight reduction in frequency for both the data of Olsen *et al.* (1973) and the present results. This is consistent with the previous observation that the average of the velocities on either side of the blunt trailing edge should be used in computing the frequency. Finally, in agreement with the present vortex-shedding results, the data of Olsen *et al.* (1973) shown in figure 1 indicate that a cut-off in lip noise tone occurs when the velocity ratio drops below 0·5.

4. Theory

Abernathy & Kronauer (1962) have shown that the vortex formation in the wake of blunt bodies can be explained by considering the nonlinear interaction of two infinite, initially parallel vortex sheets in an inviscid incompressible fluid. In their analysis, the vortex sheets were represented by two rows of point vortices that were subjected to an initial disturbance. Flow patterns based on the calculated motion of the point vortices indicated that the vortices tended to cluster and form clouds resembling the Kármán vortex street. In the Abernathy–Kronauer model, the mean flow velocities outside the vortex streets were equal. The present analysis represents an extension of the Abernathy–Kronauer model to include the effect of unequal external mean velocities on vortex formation.

The analytical model of two horizontal rows of point vortices which are separated by a distance h is illustrated in figure 4. These rows, which are initially parallel, are perturbed by a sinusoidal disturbance of wavelength a. The ensuing wave patterns assumed by the upper and lower rows of vortices for various free-

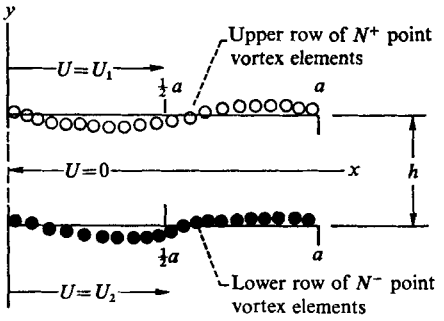

FIGURE 4. Sketch showing one wavelength of a periodic perturbation of two initially parallel infinite vortex sheets. ○, point vortex element with clockwise rotation; ●, point vortex with counterclockwise rotation.

stream velocity ratios are then calculated as a function of time. The numbers of point vortices per wavelength in the upper and lower rows are N^+ and N^-, respectively (note that hereafter the superscripts $\pm$ will be used to denote the upper and lower row, respectively). The free-stream velocities are adjusted such that U attains a value U_1 as $y \to +\infty$ and a value U_2 as $y \to -\infty$. In the region $-\frac{1}{2}h < y < \frac{1}{2}h$, the mean velocity is zero. As in the Abernathy–Kronauer analyses, only antisymmetric disturbances (symmetric disturbances shifted by one half-wavelength in one of the sheets) will be considered, since these were shown in the above reference to give the first indication of a vortex-street arrangement.

The differential equations governing the motion of the centres (x_j, y_j) of the individual point vortices in time are

$$\left.\begin{aligned} dx_j^{\pm}/dt &= u(x_j^{\pm}, y_j^{\pm}) \\ dy_j^{\pm}/dt &= v(x_j^{\pm}, y_j^{\pm}) \end{aligned}\right\} \quad (j = 1, 2, \ldots, N^{\pm}), \tag{1}$$

and (2)

with $2(N^+ + N^-)$ unknowns $x_j^{\pm}(t)$ and $y_j^{\pm}(t)$. As in Abernathy & Kronauer an initial sinusoidal distribution of point vortices is imposed at zero time:

$$x_j^{\pm}(0) = [(j-1)\,a/N^{\pm}] \pm \tfrac{1}{4}a + A \sin[2\pi(j-1)/N^{\pm}] \tag{3}$$

and

$$y_j^{\pm}(0) = \pm \tfrac{1}{2}h \pm B \sin[2\pi(j-1)/N^{\pm}], \tag{4}$$

where the constants A and B are associated with the initial disturbance.

The velocity components u and v of the individual vortex elements [(1) and (2)] are composed of an average velocity $\overline{U}$ due to the free-stream motion as well as a velocity induced by all the other vortex elements, that is

$$u(x,y) = \overline{U} + \sum_{k=1}^{N^+} u_k^+(x,y) + \sum_{k=1}^{N^-} u_k^-(x,y) \tag{5}$$

and

$$v(x,y) = \sum_{k=1}^{N^+} v_k^+(x,y) + \sum_{k=1}^{N^-} v_k^-(x,y), \tag{6}$$

where

$$u_k^{\pm}(x,y) = \pm\left[\frac{\overline{U}}{N^+ + N^-}\right]\frac{\sinh\left[2\pi(y-y_k^{\pm})/a\right]}{\cosh\left[2\pi(y-y_k^{\pm})/a\right]-\cos\left[2\pi(x-x_k^{\pm})/a\right]}, \tag{7}$$

$$v_k^{\pm}(x,y) = \mp\frac{\overline{U}}{(N^+ + N^-)} \times \frac{\sin\left[2\pi(x-x_k^{\pm})/a\right]}{\cosh\left[2\pi(y-y_k^{\pm})/a\right]-\cos\left[2\pi(x-x_k^{\pm})/a\right]} \quad (k = 1, 2, \ldots, N^{\pm}). \tag{8}$$

Equations (1)–(8) are similar to those given in Abernathy & Kronauer, but have been modified for unequal velocities over the top and bottom of the plate. The velocity $\overline{U}$ is defined as the average of the free-stream velocities over the top and bottom of the plate:

$$\overline{U} = \tfrac{1}{2}(U_1 + U_2). \tag{9}$$

The relationship between the number of vortex elements per wavelength and the velocity ratio U_r ($= U_2/U_1$) can be obtained by considering the limits of the u component of velocity as $y \to \pm\infty$. Thus we have

$$\lim_{y\to+\infty} u(x,y) = U_1 = \frac{2N^+}{N^+ + N^-}\overline{U}, \quad \lim_{y\to-\infty} u(x,y) = U_2 = \frac{2N^-}{N^+ + N^-}\overline{U}, \tag{10),(11}$$

or

$$U_r = U_2/U_1 = N^-/N^+, \tag{12}$$

Consequently, the ratio of the numbers of vortex elements per wavelength in the lower and upper row is equal to the velocity ratio U_r. In the calculations the number of vortex elements per wavelength in the upper row was held constant at $N^+ = 84$ for all values of U_r. Obviously, as U_r decreases, the total number of vortex elements decreases. When $U_r = 1{\cdot}00$, the number of vortex elements in the upper row is equal to the number in the lower row, i.e. $N^+ = N^- = 84$. In this case, the total number of differential equations [(1) and (2)] describing the motion of the vortex elements is 336, whereas at a velocity ratio of 0·25 the total number of differential equations is 210.

The solution of the system of differential equations was obtained by using a fourth-order Runge–Kutta method with a constant step size Δt, which was chosen to be $0{\cdot}056a/\overline{U}$. Although this step size is somewhat larger than the value used in the majority of the Abernathy–Kronauer calculations, it was adequate to provide good agreement with the published results for a velocity ratio of 1·0 (this can be noted by comparing figure 5 with figure 11 of Abernathy & Kronauer 1962). This larger step size permitted the calculations to be made for a velocity ratio of 1·00 (336 equations) within a practical computing time of about 14 min on a Univac 1100/42 upon limiting the non-dimensional time $t\overline{U}/a$ to a value of about 2·25. The value of $t\overline{U}/a$ corresponds to twice the value of tU/a in the notation of Abernathy & Kronauer (since $\overline{U}$ in the present model is equivalent to $2U$ in the Abernathy–Kronauer model).

All of the calculations were performed for a spacing ratio h/a of 0·281 (Kármán ratio). The constants A and B, associated with the initial disturbance, had values of $-0{\cdot}0890$ and $-0{\cdot}0749$, respectively, as in Abernathy & Kronauer (1962). Additional calculations, in which viscous effects were considered, indicated that viscosity had a negligible effect on the vortex patterns.

5. Comparison of experiment and theory

The results of the above calculations are shown in figures 5–8 as plots of the point-vortex positions (x, y) at various times $t\bar{U}/a$ for values of the velocity ratio U_r from 1·0 to 0·25. The periodic arrangement of point vortices, of which three oscillations are shown, is assumed to extend over $-\infty < x < +\infty$ at each instant of time. It should be noted that the actual vortex-shedding phenomenon of this experiment is not represented by these three oscillations, but rather by the changing point-vortex patterns at increasing values of time, which can be seen by progressing downwards in each figure. Thus the gradual accumulation of point vortices into clouds or clusters and their downstream movement with increasing time $t\bar{U}/a$ represent the experimental vortex-shedding phenomenon relevant to this investigation.

An examination of the theoretically computed vortex displacements as a function of time and velocity in figures 5–8 shows trends which agree in many respects with the experimental observations. First, the results in these figures show that when the velocity ratio is reduced the rate of cloud formation in the lower row is also reduced and the clouds which form in the upper row become more and more diffuse. These diffuse regions of vorticity moving in random directions take on the appearance of random turbulent motion much more than the more concentrated vortex clouds. This is consistent with the experimental observation that the vortex clouds became more indistinct as the velocity ratio was dropped, with the lower row disappearing faster than the upper.

The results for a velocity ratio of unity (figure 5) show an equal tendency in the upper and lower vortex rows to roll up and form clusters or clouds of concentrated vorticity, which form the characteristic elements of the classical Kármán vortex street. A comparison of the results for a velocity ratio of unity with those for other velocity ratios indicates a less rapid broadening of the wake as the velocity ratio is reduced for any given value of the non-dimensional time parameter $t\bar{U}/a$. This result is in good agreement with the observations based on the smoke-study photographs in figure 3.

The calculated results also exhibit an increasing tendency of the lower clouds to fall behind and eventually be overtaken by the upper clouds. The same observation was made earlier in discussing the experimental results. Thus there is no equilibrium position of the lower clouds relative to the upper for a velocity ratio other than unity, and the conventional steady symmetric vortex-cloud spacing characteristic of the Kármán vortex street is no longer possible. When the velocity ratio is not too different from unity, this lack of symmetry can be accommodated by diffusion of the vortex cloud. But when the velocity ratio gets too low, the lack of symmetry will cause the disappearance of the stable vortex clouds that was noted in both the experimental smoke studies and the coaxial-nozzle noise studies of Olsen *et al.* (1973).

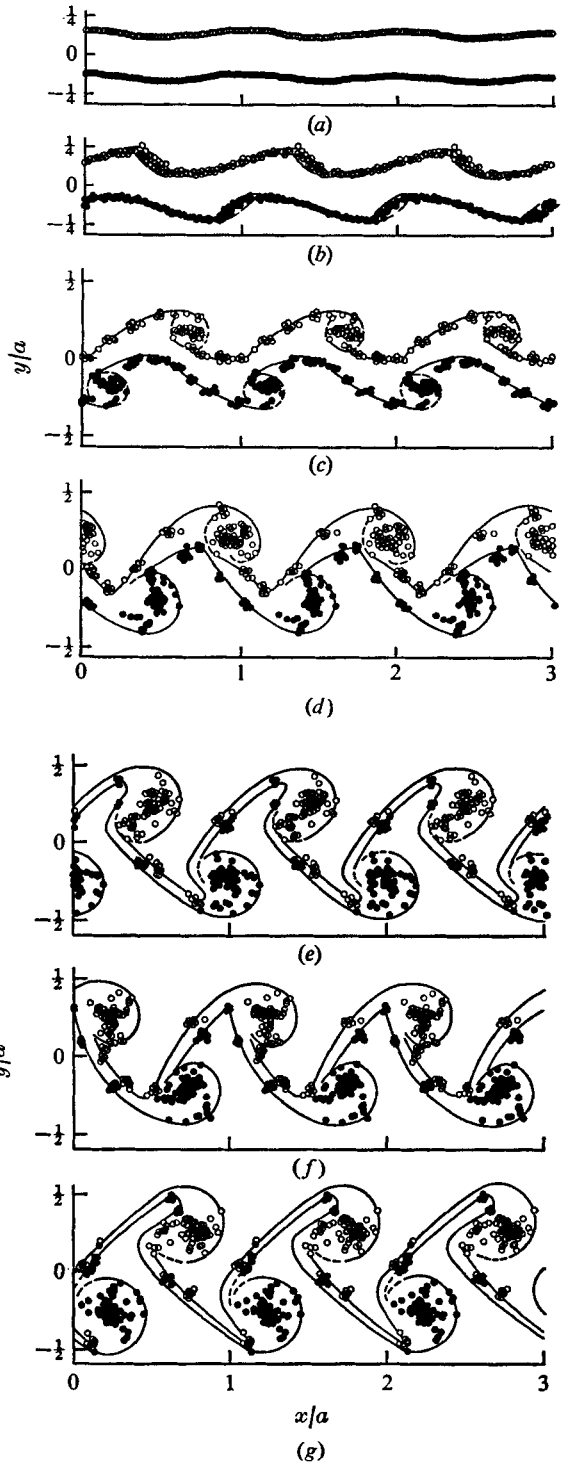

FIGURE 5. Point-vortex patterns at a velocity ratio $U_r = 1{\cdot}0$; $h/a = 0{\cdot}281$, $\bar{U} = 1{\cdot}0$, $A = -0{\cdot}0890$, $B = -0{\cdot}0749$, $N^+ = 84$, $N^- = 84$. (*a*) Time $t\bar{U}/a = 0$. (*b*) $t\bar{U}/a = 0{\cdot}394$. (*c*) $t\bar{U}/a = 0{\cdot}786$. (*d*) $t\bar{U}/a = 1{\cdot}180$. (*e*) $t\bar{U}/a = 1{\cdot}573$. (*f*) $t\bar{U}/a = 1{\cdot}910$. (*g*) $t\bar{U}/a = 2{\cdot}248$.

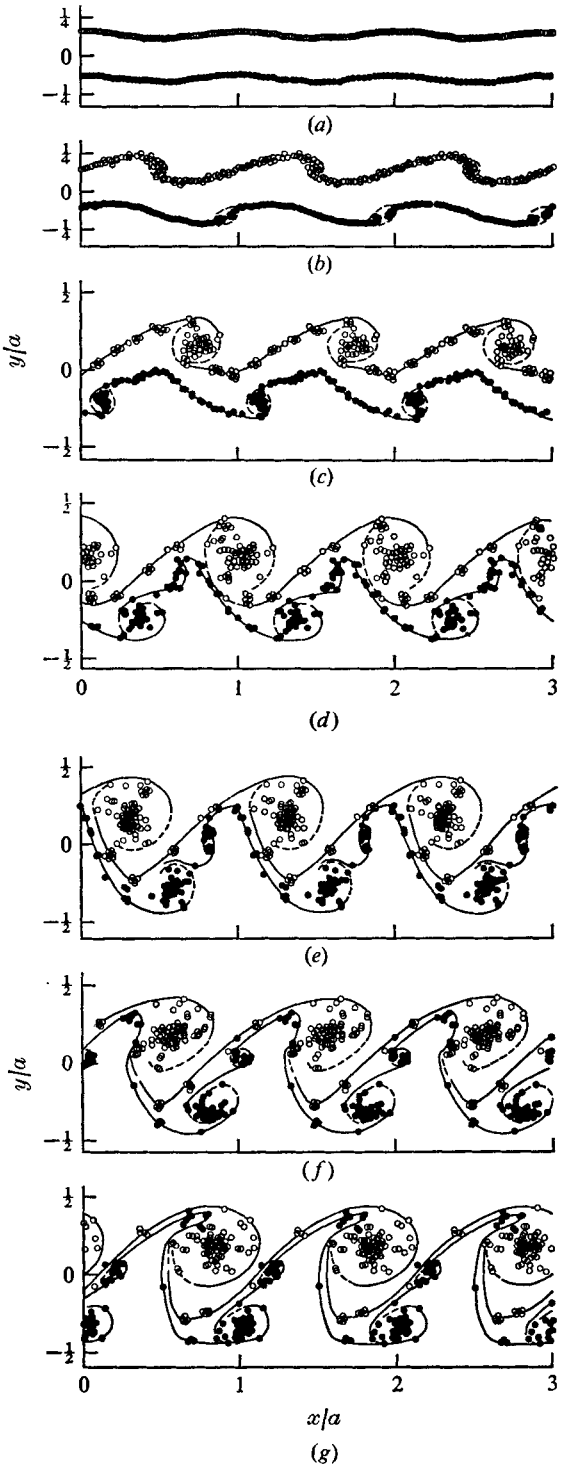

FIGURE 6. Point-vortex patterns at a velocity ratio $U_r = 0{\cdot}75$; $h/a = 0{\cdot}281$, $\bar{U} = 1{\cdot}0$, $A = -0{\cdot}0890$, $B = -0{\cdot}0749$, $N^+ = 84$, $N^- = 63$. (*a*)–(*g*) as in figure 5.

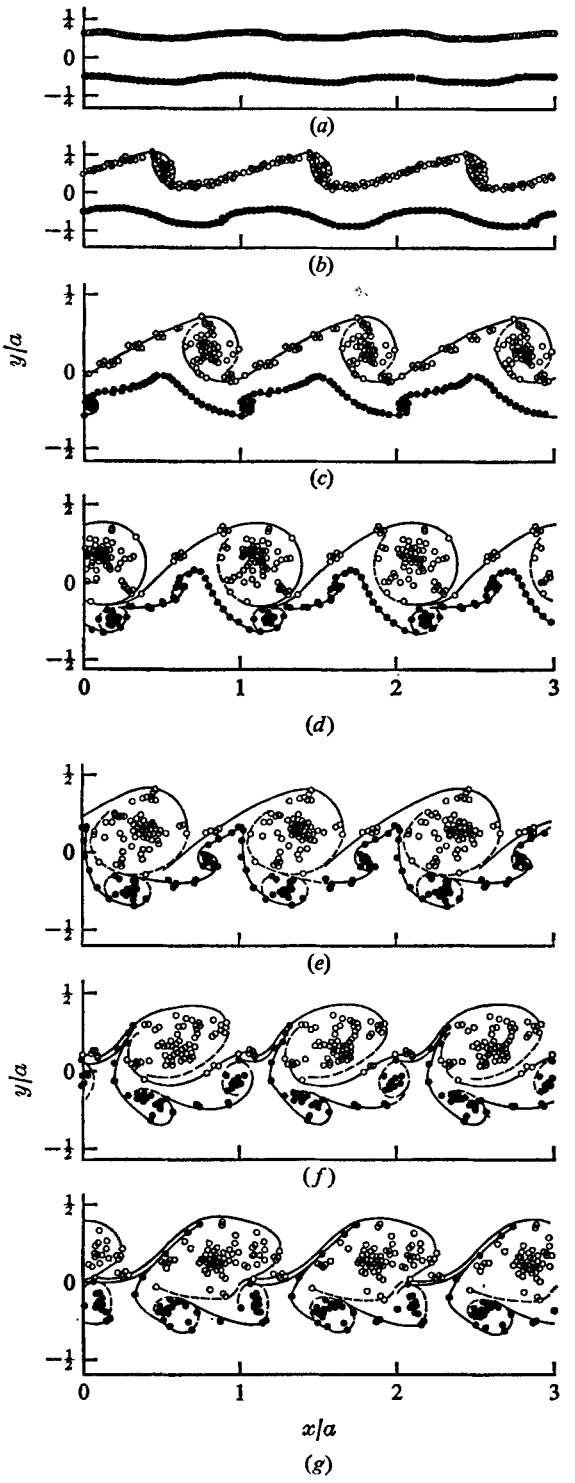

FIGURE 7. Point-vortex patterns at a velocity ratio $U_r = 0{\cdot}5$; $h/a = 0{\cdot}281$, $\bar{U} = 1{\cdot}0$, $A = -0{\cdot}0890$, $B = -0{\cdot}0749$, $N^+ = 84$, $N^- = 42$. (*a*)–(*g*) as in figure 5.

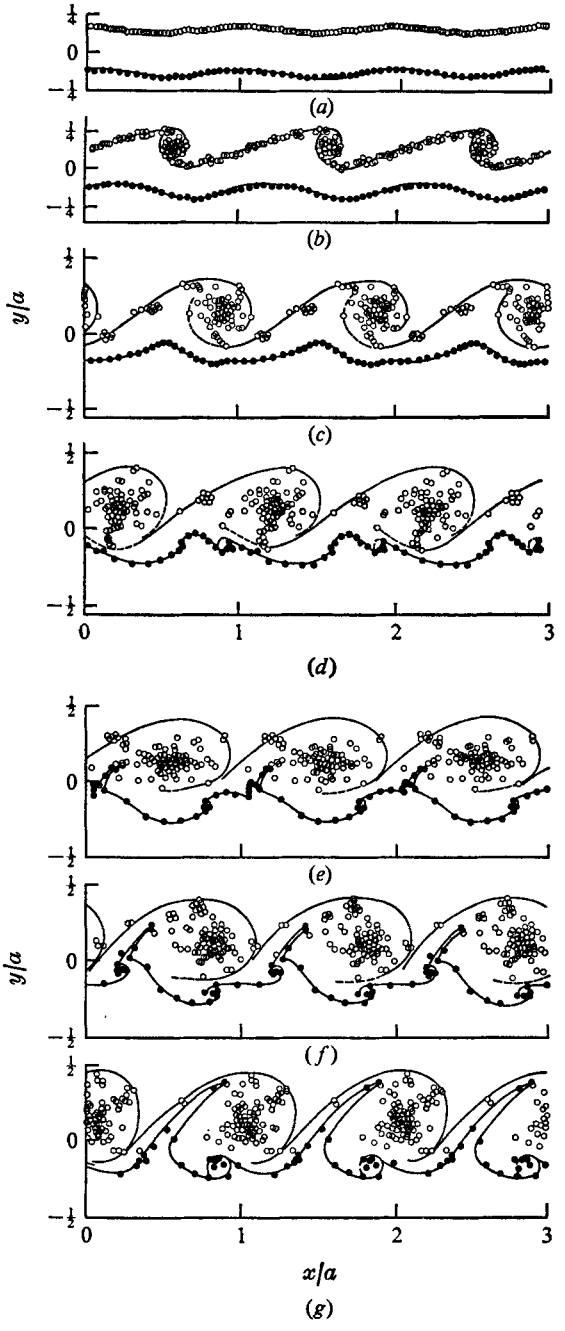

FIGURE 8. Point-vortex patterns at a velocity ratio $U_r = 0{\cdot}25$; $h/a = 0{\cdot}281$, $\overline{U} = 1{\cdot}0$, $A = -0{\cdot}0890$, $B = -0{\cdot}0749$, $N^+ = 84$, $N^- = 21$. (*a*)–(*g*) as in figure 5.

Velocity ratio U_2/U_1	Experiment V_1/U_1 (using figure 3; smoke)	Analysis V_1/U_1 (using figures 5–8)	Analysis V_2/V_1 (using figures 5–8)
1·0	0·71	0·70	1·0
0·75	0·59	0·65	0·78
0·5	0·59	0·55	0·48
0·25	Undetectable	0·50	0·23–0·55

TABLE 2. Relative velocities of vortex clouds

As indicated in the earlier discussion of the smoke photographs, convection velocities of the upper vortex street were measured. Likewise, convection velocities of vortex clouds were inferred from the theoretical vortex patterns shown in figures 5–8. This was done by noting the x location of a given vortex cloud at each of the specified times and dividing the change in location by the time interval. Establishing the location of a vortex cloud involved judging which point vortices belong to a cloud and then assigning an approximate centre to the cloud. With the velocity of the upper vortex cloud designated by V_1 and that of the lower by V_2, the measured velocities are shown in table 2, together with those obtained from the movie film.

A comparison of the second and third columns indicates approximate agreement between experiment and theory for the ratio V_1/U_1 of the velocities of the upper vortex cloud and the upper stream. Because of the difficulty of determining vortex-cloud centres from the smoke photographs, it was even more difficult to determine vortex-cloud velocities for the experiments than it was for the theoretical vortex-cloud developments in figures 5–8. Hence a more exact agreement should not be expected.

The last column in table 2 is the ratio of the velocity V_2 of the lower vortex cloud to the velocity V_1 of the upper cloud as determined from figures 5–8. The excellent agreement between V_2/V_1 and U_2/U_1 for the first three cases indicates that the vortex clouds progress downstream at the same fraction of the free-stream velocity for both the upper and lower vortex row, i.e. $V_1/U_1 = V_2/U_2$.

The development of the vortex street for the $U_2/U_1 = 0{\cdot}25$ case in figure 8 shows a much diminished tendency of the lower vortices to form well-defined clouds compared with the higher velocity ratios. Also, an estimate of the ratio V_2/V_1 of what appear to be lower-cloud and upper-cloud velocities is not necessarily the same as the ratio of the free-stream velocities U_2/U_1 as was the case for the larger velocity ratios. The values $V_2/V_1 = 0{\cdot}23$ and 0·55 in table 2 are average values obtained for the two lower groups of points, which resemble loosely defined clouds.

6. Concluding remarks

The study of the turbulent flow behind a blunt trailing edge with unequal external mean velocities revealed the following.

(i) Smoke-study data indicated that the periodic vortex shedding which was evident at a velocity ratio of 1·0 tended to become less distinct and eventually disappeared as the velocity ratio U_2/U_1 approached zero. These observations provided an explanation for the phenomenon referred to as 'lip noise' often observed in coaxial jets. The experiment showed that a Strouhal number of about 0·2, based on the lip thickness and a mean velocity $\overline{U}$, was associated with both vortex shedding and lip noise.

(ii) Theoretical calculations of the vortex formation based on an incompressible inviscid model of the vortex street were in good agreement with the experiment. The calculated wake flow patterns showed that as the velocity ratio was reduced there was a weaker tendency for clouds to form in the lower row (corresponding to the lower external mean velocity) and that the clouds in the upper row became more diffuse, thus suggesting random turbulent motion. Also, as the velocity ratio approached unity the clouds became more and more concentrated; this behaviour was also verified by experiment.

REFERENCES

ABERNATHY, F. H. & KRONAUER, R. E. 1962 The formation of vortex streets. *J. Fluid Mech.* **13**, 1–20.

HERZIG, H. A., HANSEN, A. G. & COSTELLO, G. R. 1954 A visualization study of secondary flow in cascades. *N.A.C.A. Tech. Rep.* no. 1163.

OLSEN, W. A., GUTIERREZ, O. A. & DORSCH, R. G. 1973 The effect of nozzle inlet shape, lip thickness, and exit shape and size on subsonic jet noise. *A.I.A.A. Paper*, no. 73-187.

OLSEN, W. & KARCHMER, A. 1976 Lip noise generated by flow separation from nozzle surfaces. *A.I.A.A. Paper*, no. 76-3.

SCHLICHTING, H. 1960 *Boundary Layer Theory.* McGraw-Hill.

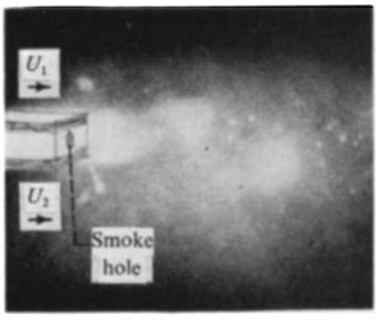

(*a*)

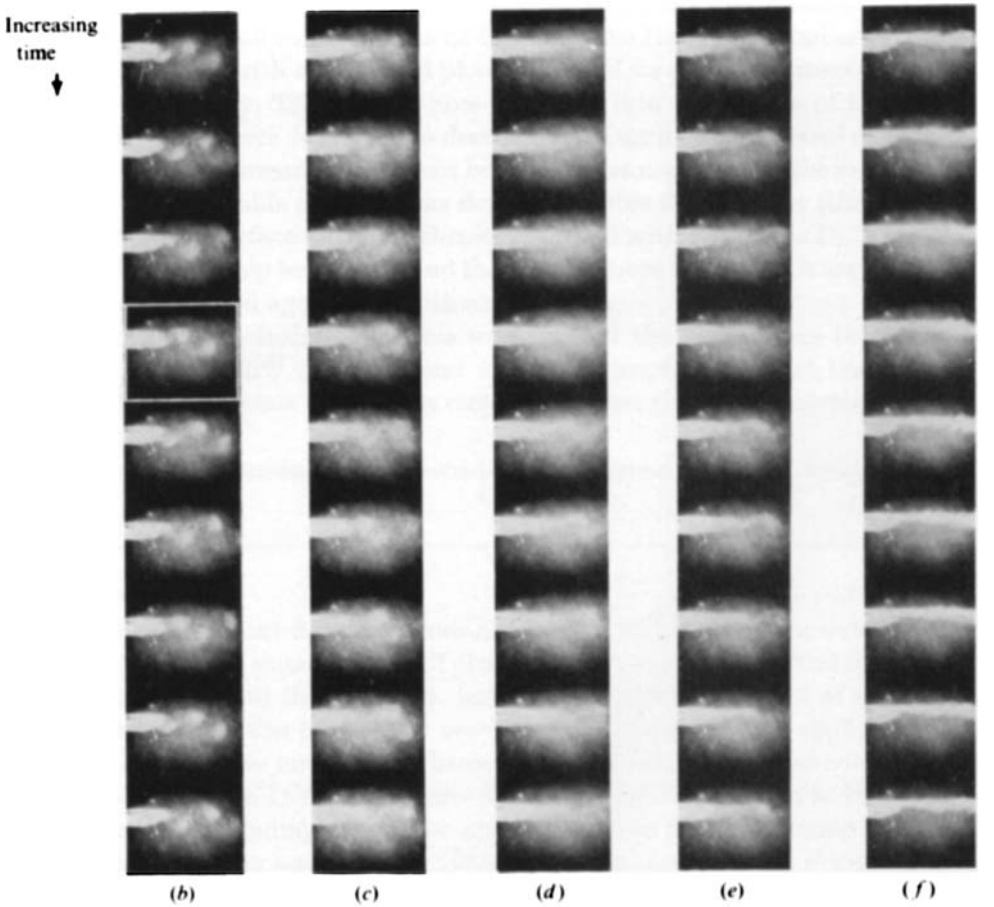

FIGURE 3. Wake-flow motion-picture sequences at various velocity ratios ($U_r = U_2/U_1$). (*a*) Magnification of single frame to show detail near blunt trailing edge. (*b*) $U_r = 1{\cdot}0$. (*c*) $U_r = 0{\cdot}75$. (*d*) $U_r = 0{\cdot}5$. (*e*) $U_r = 0{\cdot}25$. (*f*) $U_r = 0$.